scientific reports

OPEN Finite element simulations of hybrid nano-Carreau Yasuda fluid with hall and ion slip forces over rotating heated porous cone

Umar Nazir[1], Muhammad Sohail[1✉], Mahmoud M. Selim[2,3], Hussam Alrabaiah[4,5] & Poom Kumam[6,7✉]

Involvement of hybrid nanoparticles a vital role to improve the efficiency of thermal systems. This report covers the utilization of different nanoparticles mixed in Carreau Yasuda material for the improvement of thermal performance. The configuration of flow situation is considered over a rotating porous cone by considering the Hall and Ion slip forces. Transport of momentum is considered to be in a rotating cone under generalized ohm's law and heat transfer is presented by considering viscous dissipation, Joule heating and heat generation. Rheology of considered model is derived by engaging the theory proposed by Prandtl. Modeled complex PDEs are reduced into ODEs under similarity transformation. To study the physics behind this phenomenon, solution is essential. Here, FEM (Finite Element Method) is adopted to compute the solution. Furthermore, the grid independent study is reported with several graphs and tables which are prepared to note the influence of involved parameters on thermal and velocity fields. It is worth mentioning that heat transport is controlled via higher radiation parameter and it upsurges for Eckert number. Moreover, Hall and ion slip parameters are considered significant parameters to produce the enhancement in motion of fluid particles but speed of nano and hybrid nanoparticles becomes slow down versus large values of Forchheimer and Weissenberg numbers. Additionally, an enhancement in production of heat energy is addressed via large values of heat generation number and Eckert number while reduction in heat energy is occurred due to positive values of thermal radiation and Hall and ion slip parameters.

Flow over a rotating geometries got considerable attention by the researchers due to their wider applications in numerous technological developments instruments and appliances. Inclusion/mixing of hybrid nanoparticles is highly recommended by the engineers to improve the thermal performance. Many rheological relations have been proposed by the researchers to study transport phenomenon. An important relation of Carreau-Yasuda model[1–5] is

$$\eta_{CY}(\dot{\gamma}) = \mu_\infty + (\mu_0 - \mu_\infty)\left[1 + (\Upsilon\dot{\gamma})^d\right]^{\frac{n-1}{d}}.$$

For $\Upsilon = 0$ or $n = 1$, Newtonian model is recovered. Due to diverse applications, this model got the remarkable attention and attraction by different researchers. For instance, Mahmood et al.[1] presented the finite element based computational analysis on Carreau-Yasuda model in a cavity with obstacle. They plotted the behavior of influential fluid parameters and analyzed the tabular results for comparison purpose. They noted the depreciation

[1]Department of Applied Mathematics and Statistics, Institute of Space Technology, P.O. Box 2750, Islamabad 44000, Pakistan. [2]Department of Mathematics, Al-Aflaj College of Science and Humanities Studies, Prince Sattam Bin Abdulaziz University, Al-Aflaj 710-11912, Saudi Arabia. [3]Department of Mathematics, Suez Faculty of Science, Suez University, Suez 34891, Egypt. [4]College of Engineering, Al Ain University, Al Ain, UAE. [5]Department of Mathematics, Tafila Technical University Tafila, At-Tafilah, Jordan. [6]Center of Excellence in Theoretical and Computational Science (TaCS-CoE) and KMUTT Fixed Point Research Laboratory, Room SCL 802 Fixed Point Laboratory, Science Laboratory Building, Departments of Mathematics, Faculty of Science, King Mongkut's University of Technology Thonburi (KMUTT), 126 Pracha-Uthit Road, Bang Mod, Thung Khru, Bangkok 10140, Thailand. [7]Department of Medical Research, China Medical University Hospital, China Medical University, Taichung 40402, Taiwan. ✉email: muhammad_sohail111@yahoo.com; poom.kum@kmutt.ac.th

in viscosity of Carreau-Yasuda material by improving the relaxation time. Steady and oscillatory flow behavior of Carreau-Yasuda material via Lattice Boltzmann procedure (LBP) was reported by Boyd and Buick[2]. They discovered the different behavior in flow of Carreau-Yasuda material under different situations and assumptions. Coclite et al.[3] analyzed different impacts of Carreau-Yasuda material in a lid-driven cavity. Stability analysis for Carreau-Yasuda material obeying poiseulle flow phenomenon via Chebyshev polynomial tool (CPT) was explored by Pinarbasi and Liakopoulos[4]. Bio-convection phenomenon in radiated chemically reactive magnetized slip of Carreau-Yasuda material was examined by Waqas et al.[5]. They engaged BVP4C package (MATLAB COMPUTATIONAL PACKAGE) to compute solution of transformed modeled problem. Several important flow features have been captured against numerous influential parameters. Results have been compared as a limiting case current inspection with the published ones. They observed the decline in fluid velocity against Rayleigh number and it escalates for Weissenberg parameter. Also, augmentation in thermal field is recorded against slip parameter.

Thermal stability and mechanism of heat transportation is essential to study the thermal performance of nanoparticles. Researchers have presented several models for the therrmophysical features of nanoparticles and recorded their advantages and disadvantages. Inclusion of nanoparticles is a hot topic of research because of their vast applications. One cannot avoid the use of nanoparticles. These coated particles are used in different appliances and medical instruments for the treatment of patients suffering in different diseases. Several researchers paid attention on this direction. For instance, Darcy-Forchheimer flow of convective carbon water based nanofluid immersed in a stretching cylinder with viscous dissipation, radiation, variable thermal conductivity and obeying slip constraints was analyzed by Hayat et al.[6] by engaging the model of thermophysical features proposed by Xue. Solution to the governing modeled expressions has been approximated by shooting procedure. They recorded the dual behavior of velocity and temperature fields against curvature parameter. Moreover, heat transportation rate escalates against radiation parameter, whereas depreciation in skin friction is noted for growing Eckert number. Electrically conducting radiative stretched flow of convective incompressible nanofluid with variable magnetic field was studied by Nayak et al.[7] via shooting procedure. They presented the validation of obtained solution by comparing the results. They recorded the diminution in thermal field for higher convection parameter. Hady et al.[8] presented the comparative analysis for convective nonlinear flow saturated in permeable surface via numerically procedure. They displayed several results against numerous influential parameters. They found the decrease in heat transportation rate for higher porosity parameter and an increase in skin friction. Nonlinear chemically reactive flow of Maxwell nanofluid past over a rotating stretched surface with activation energy was explored by Shafique et al.[9]. They used shooting method to obtain the solution of boundary layer transformed ODEs. They observed the influence of several emerging parameters through graphs and tabular data. They noted the enhancement in mass transfer rate for Schmidt number and depreciation in concentration field. Utilization of SWCNTs and MWCNTs to improve the thermal performance of engine oil and water based rotating viscous liquid with internal heating was examined by Rehman et al.[10]. They solved the resulting equations numerically and flow behavior is monitored through graphs and tabular data. They analyzed the higher skin friction and heat transfer rate for engine oil based mixture as compared with water based mixture for both MWCNTs and SWCNTs. Moreover, significant escalation in velocity field is recorded for higher volume fraction. Seth et al.[11] worked on nonlinear mixed convective flow of viscous liquid past over a nonlinear stretched surface via FEM and OHAM. They considered velocity slip and performed regression analysis. They noticed the increase in velocity for stagnation parameter and decrease in thermal profile. Kandasamy et al.[12] developed alumunia and copper based model to notice the thermal performance of mixed convective chemically reactive flow. They used the thermophysical model proposed by Magyari and Mamut. They noticed the several important features through plots. They monitored the rise in velocity for velocity slip parameter and opposite trend in concentration field. McCash et al.[13] studied characteristics of viscous fluid inside two tubes using exact solution approach. Zidan et al.[14] discussed the thermal aspects of blood flow in multiple stenosis. They used exact approach to know behavior of blood flow and entropy generation. Saleem et al.[15] performed bio-mathematical scheme to know behavior of blood flow in artery (non-symmetric and symmetric stenosed) including Joule heating. McCash et al.[16] modeled flow behavior of Peristaltic liquid inserting hybrid nanoparticles in an Elliptic Duct along with advancing boundaries. Rehman et al.[17] highlighted thermal aspects in pseudoplastic liquid inserting nanoparticles over Riga heated surface considering thermophoresis diffusion and Brownian motion. They estimated surface force, flow and heat energy using various physical parameters and numerically solved by numerical scheme. Akhtar et al.[18] discussed features of heat energy in non-Newtonian fluid including carbon nanotubes towards. They used exact solution scheme to know aspects of pressure gradient, heat energy and flow phenomena inside melting a vertical duct. Rizwana et al.[19] scrutinized formulation of thermal aspects under the action of magnetic field over oscillating melting plate inserting nanoparticles along with convective boundary conditions. Yasin et al.[20] discussed laminar flow in heated rods via finite element method approach. Ahmad et al.[21] formulated micropolar liquid suspending hybrid nanoparticles using non-Fourier's theory considering triple stratification. Yasin et al.[22] used finite element approach to know aspects of Lorentz forces along with convective flow in adiabatic (enclosure). Hussain et al.[23] formulated heat transfer in Carreau–yasuda liquid inserting nanoparticles towards melting surface. Nazir et al.[24] simulated comparative results of hybrid nanoparticles in Williamson among nanoparticles and hybrid nanoparticles towards a meeting sheet using non-Fourier's theory. In another survey, Nazir et al.[25] discussed comparison analysis in Carreau liquid among variable and constant viscosity via non-Fourier's theory numerically solved by FEA (finite element approach). Important studies contributing the modeling of several phenomena under different flow conditions are reported in[26–31].

Available literature has no reported study by considering the inclusion of hybrid nanoparticles in Carreau-Yasuda model with dissipation effect and engagement of Hall and ion slip forces in rotating porous cone. This report will be used as a base for the researchers working further on Carreau-Yasuda model by engaging different physical effects. This draft is organized as: comprehensive literature survey is included in Sect. 1, modeling

is mentioned in Sect. 2 along with important physical quantities, Sect. 3 contains the explanation of solution scheme, graphical and tabular results are reported in Sect. 4 and important results have been listed in Sect. 5.

In future endeavors this work will be extended by considering following important effects.

- Slip effects, variable viscosity (space dependent/shear rate dependent/concentration dependent/temperature dependent) and variable magnetic field;
- Mixed convection;
- Modified heat flux and radiation effect;
- Variable thermal conductivity;
- Space dependent heat source;
- Variable diffusion coefficient;
- Utilization of ternary hybrid nanoparticles mixture;
- Linear, nonlinear stretching sheets with and without porosity;
- CPU analysis of iteration of different schemes and comparative study.

Nomenclature

Symbols/units	Used for	Symbols/units	Used for
z, x, y[m]	Space coordinates	Ec[no unit]	Eckert number
u, v, w[ms^{-1}]	Velocity components	Re[no unit]	Reynolds number
G[Newton]	Gravitational force	nf	Nano-fluid
U_w[ms^{-1}]	Wall velocity	We[no unit]	Weissenberg number
T[kelvin]	Temperature field	H_s	Heat generation number
T_∞, T_w[kelvin]	Ambient and wall temperatures	Nu	Nusselt number
B_0[Oersted Ampere/meter]	Magnetic field strength	SiO_2	Silicon dioxide
C_f, C_g	Skin friction coefficients	T_0[kelvin]	Reference temperature
k[(W/(m·K))]	Thermal conductivity	Greek symbols	
hnf, bf	Hybrid nanofluid and base fluid	α[radian]	Semi vehicle angle
C_p[J kg^{-1} K^{-1}]	Specific heat capacity	β_i, β_e	Ion slip and Hall forces
g, f	Velocity components	ϕ, ϕ_2, ϕ_1	Volume fractions
M^2	Magnetic field	θ	Temperature
Pr[no unit]	Prandtl number	η	Independent variable
l[m]	Characteristic length	τ_{xz}	Wall shear stress
n	Power law index number	λ	Mixed convection parameter
d	Carreau Yasuda fluid number	Ω	Radial velocity
F_s	Inertia cofficient	ν m^2 s^{-1}	Kinematic viscosity
F_r	Forchheimer number	ρ[kg m^{-3}]	Fluid density
N_r	Thermal radiation number	μ[kg m^{-1} s^{-1}]	Viscosity
$C_2H_6O_2$	Ethylene glycol	σ[Sm^{-1}]	Electrical conductivity
MoS_2	Molybdenum dioxide	Γ	Time constant
PDEs	Partial differential equations	ϵ	porosity number

Formulation of heat transport model

The simulations of transport of heat energy involving the dispersion of MoS_2 and SiO_2 called hybrid nanofluid in Carreau Yasuda liquid past a porous rotating cone with variable wall temperate are performed. Physically, the rotation in flow of hybrid nanoparticles is occurred due to rotating of a cone while Hall and ion-slip currents are taken into account. The heated cone is designed as space coordinates (x, y, z) are taken along u, v and w whereas x-axis is known as tangential direction, azimuthal and normal directions are called y- and z-axis. The bouncy forces are appeared due to gravitational force. Moreover, the impacts of Darcy's porous medium, Joule heating, viscous dissipation, thermal radiation and heat generation are modeled. The composition of MoS_2 and SiO_2 is called hybrid nanoparticles while MoS_2 is named as nanoparticles in base liquid (ethylene glycol). Physical flow transport phenomena are illustrated by Fig. 1. The sketching view of hybrid nanoparticles is considered by Fig. 2. Thermal properties of hybrid nanoparticles is mentioned in table 1. The non-linear PDEs[32,33] are developed using BLAs (boundary layer approximations) and present flow phenomena in mathematical mode is established as

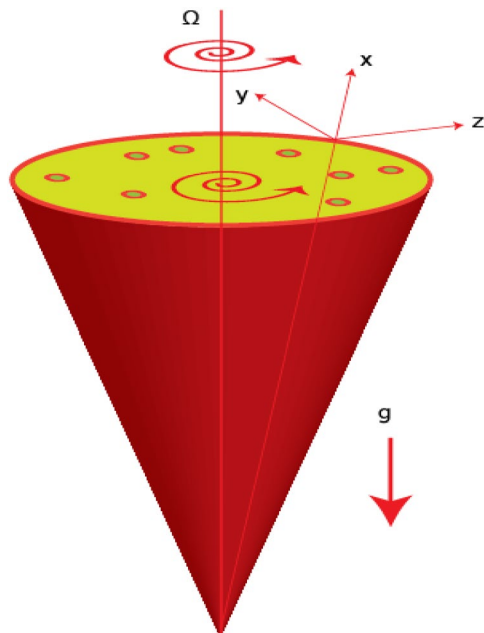$$\frac{\partial(xu)}{\partial x} + \frac{\partial(xv)}{\partial z} = 0,$$ (1)

Figure 1. Flow behavior of hybrid nanoparticles.

MoS_2/SiO_2	$C_2H_6O_2$	MoS_2
$\rho_{MoS_2/SiO_2} = 5060$	$\rho_{C_2H_6O_2} = 1113.5$	$\rho_{MoS_2} = 2650$
$\left(C_p\right)_{MoS_2/SiO_2} = 397.746$	$\left(C_p\right)_{C_2H_6O_2} = 2430$	$\left(C_p\right)_{MoS_2} = 730$
$k_{MoS_2/SiO_2} = 34.5$	$k_{C_2H_6O_2} = 0.253$	$k_{MoS_2} = 1.5$
$\sigma_{MoS_2/SiO_2} = 1 \times 10^{-18}$	$\sigma_{C_2H_6O_2} = 4.3 \times 10^{-5}$	$\sigma_{MoS_2} = 0.0005$

Table 1. Thermal properties of hybrid nanoparticles with base fluid.
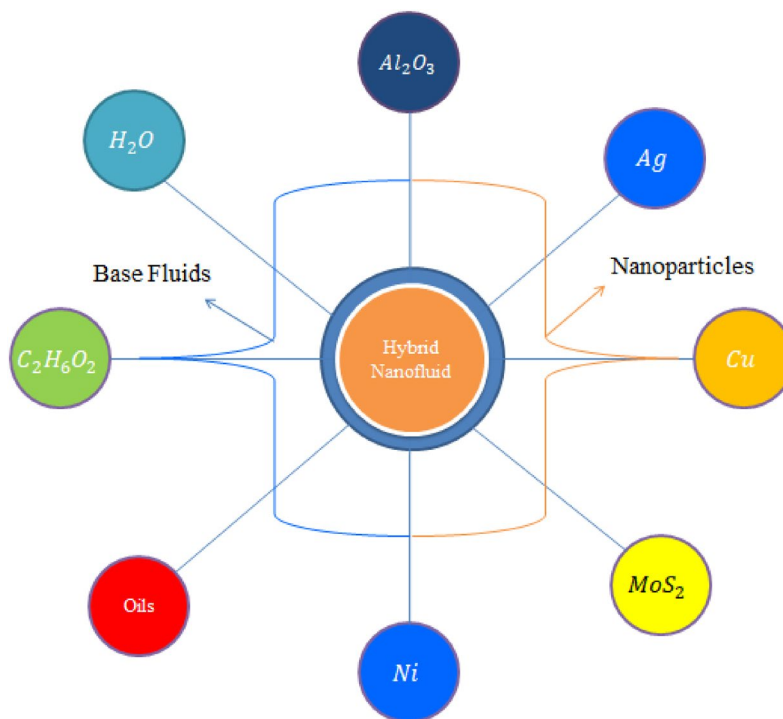
Figure 2. The sketching behavior of hybrid nanoparticles.

$$u\frac{\partial u}{\partial x} + w\frac{\partial u}{\partial z} = \frac{v^2}{x} + \nu_{hnf}\left[\frac{\partial^2 u}{\partial z^2} + \Gamma^d\left(\frac{n-1}{d}\right)(d+1)\frac{\partial^2 u}{\partial z^2}\left(\frac{\partial u}{\partial z}\right)^d\right] + G\beta(T-T_\infty)cos\alpha \left.\right\}$$
$$+ \frac{B_0^2\sigma_{hnf}}{\rho_{hnf}\left[(1+\beta_e\beta_i)^2+\beta_e^2\right]}[\nu\beta_e - (1+\beta_e\beta_i)u] - \frac{\nu_{hnf}}{k^*}F_s u - \frac{F_s}{(k^*)^{1/2}}u^2 \qquad (2)$$

$$u\frac{\partial v}{\partial x} + w\frac{\partial v}{\partial z} = \frac{uv}{x} + \nu_{hnf}\left[\frac{\partial^2 v}{\partial z^2} + \Gamma^d\left(\frac{n-1}{d}\right)(d+1)\frac{\partial^2 v}{\partial z^2}\left(\frac{\partial v}{\partial z}\right)^d\right] \left.\right\}$$
$$- \frac{B_0^2\sigma_{hnf}}{\rho_{hnf}\left[(1+\beta_e\beta_i)^2+\beta_e^2\right]}[u\beta_e + (1+\beta_e\beta_i)v] - \frac{\nu_{hnf}}{k^*}F_s v - \frac{F_s}{(k^*)^{1/2}}v^2 \qquad (3)$$

$$u\frac{\partial T}{\partial x} + w\frac{\partial T}{\partial z} = \frac{k_{hnf}}{(\rho c_p)_{hnf}}\left[\frac{\partial^2 T}{\partial z^2} + \frac{\sigma^* 16 T_\infty^3}{3k^*}\frac{\partial^2 T}{\partial z^2}\right] + \frac{B_0^2\sigma_{hnf}}{\rho_{hnf}\left[(1+\beta_e\beta_i)^2+\beta_e^2\right]}\left(u^2+v^2\right) \left.\right\}$$
$$+ \frac{\mu_{hnf}}{(\rho C_p)_{hnf}}\left[1+\left\{(\Gamma)^d\left(\frac{n-1}{d}\right)\right\}\left(\frac{\partial u}{\partial z}\right)^d + \left(\frac{\partial v}{\partial z}\right)^d\right]\left[\left(\frac{\partial u}{\partial z}\right)^2 + \left(\frac{\partial v}{\partial z}\right)^2\right] + Q_0(T-T_\infty) \qquad (4)$$

The BCs (boundary conditions)[32] are simulated using concept of no-slip theory

$$\left.\begin{array}{l} u=0, v=\Omega x sin\alpha, T=T_w, w=0 \text{ at } z=0 \\ u\to 0, v\to 0, T\to T_\infty \text{ at } z\to\infty \end{array}\right\}. \qquad (5)$$

The change of variables are constructed as

$$\left.\begin{array}{l} u=-\frac{\Omega x sin\alpha}{2}f', v=\Omega x sin\alpha g, w=\left(\Omega \nu_f sin\alpha\right)^{\frac{1}{2}}f \\ \theta=\frac{T-T_\infty}{T_w-T_\infty}, \eta=z\sqrt{\frac{\Omega sin\alpha}{\nu_f}}, T_w=T_\infty+\frac{x(T_0-T_\infty)}{l} \end{array}\right\}. \qquad (6)$$

The correlations of thermo-physical properties in nano and hybrid nanoparticles are

$$\left.\begin{array}{l} \rho_{nf}=(1-\phi)\rho_f+\phi\rho_s, \ \rho_{hnf}=\left[(1-\phi_2)\{(1-\phi_1)\rho_f+\phi_1\rho_{s_1}\}\right]+\phi_2\rho_{s_2} \\ (\rho C_p)_{nf}=(1-\phi)(\rho C_p)_f+\phi(\rho C_p)_s, \ (\rho C_p)_{hnf}=\left[(1-\phi_2)\{(1-\phi_1)(\rho C_p)_f+\phi_1(\rho C_p)_{s_1}\}\right] \\ +\phi_1(\rho C_p)_{s_2} \end{array}\right\}, \qquad (7)$$

$$\left.\begin{array}{l} \mu_{nf}=\frac{\mu_f}{(1-\phi)^{2.5}}, \ \mu_{nf}=\frac{\mu_f}{(1-\phi_2)^{2.5}(1-\phi_1)^{2.5}}, \ \frac{k_{nf}}{k_f}=\left\{\frac{k_s+(n+1)k_f-(n-1)\phi(k_f-k_s)}{k_s+(n-1)k_f+\phi(k_f-k_s)}\right\} \\ \frac{k_{hnf}}{k_{bf}}=\left\{\frac{k_{s_2}+(n-1)k_{bf}-(n-1)\phi_2(k_{bf}-k_{s_2})}{k_{s_2}+(n-1)k_{bf}-\phi_2(k_{bf}-k_{s_2})}\right\}, \ \frac{\sigma_{hnf}}{\sigma_f}=\left(1+\frac{3(\sigma-1)\phi}{(\sigma+2)-(\sigma-1)\phi}\right) \\ \frac{\sigma_{hnf}}{\sigma_f}=\left(\frac{\sigma_{s_2}+2\sigma_f-2\phi_2(\sigma_{bf}-\sigma_{s_2})}{\sigma_{s_2}+2\sigma_f+\phi_2(\sigma_{bf}-\sigma_{s_2})}\right), \ \frac{\sigma_{bf}}{\sigma_f}=\left(\frac{\sigma_{s_1}+2\sigma_f-2\phi_1(\sigma_f-\sigma_{s_1})}{\sigma_{s_1}+2\sigma_f+\phi_1(\sigma_f-\sigma_{s_1})}\right) \end{array}\right\} \qquad (8)$$

Equations (1–5) are transformed into dimensionless Eqs. (7–9) using Eq. (6)

$$\left.\begin{array}{l} f''' + \frac{\nu_f}{\nu_{hnf}}\left(\frac{1}{2}(f')^2 - ff'' - 2g^2 - 2\lambda\theta\right) - \frac{M^2(1-\phi_1)^{2.5}(1-\phi_2)^{2.5}}{(1+\beta_e\beta_i)^2+\beta_e^2}\left[2\beta_e g + (1+\beta_e\beta_i)f'\right] \\ +(We)^d\frac{(n-1)(d+1)}{d}f'''(f'')^d + \epsilon f' - H_1 F_r(f')^2 = 0, \\ f(0)=f'(0)=0, \ f'(\infty)=0, \end{array}\right\} \qquad (9)$$

$$\left.\begin{array}{l} g'' + \frac{\nu_f}{\nu_{hnf}}\left(gf'-fg'\right) - \frac{M^2(1-\phi_1)^{2.5}(1-\phi_2)^{2.5}}{(1+\beta_e\beta_i)^2+\beta_e^2}\left[-\frac{1}{2}\beta_e f' + (1+\beta_e\beta_i)g\right] \\ +(We)^d\frac{(n-1)(d+1)}{d}g''(g')^d - \epsilon g - H_1 F_r(g)^2 = 0, \\ +g(0)=1, \theta(\infty)=0, \end{array}\right\} \qquad (10)$$

$$\left.\begin{array}{l} \left(1+\frac{4}{3N_r}\right)\theta'' + \frac{k_f}{k_{hnf}}\frac{(\rho c_p)_{hnf}}{(\rho c_p)_f}Pr\left(\frac{1}{2}f'\theta - f\theta'\right) + \frac{k_f}{k_{hnf}}\frac{(1-\phi_1)^{-2.5}PrEcM^2}{(1-\phi_2)^{2.5}[(1+\beta_e\beta_i)^2+\beta_e^2]}\left[\frac{1}{4}(f')^2 + (g)^2\right] \\ \frac{k_f}{k_{hnf}}\frac{PrEc}{(1-\phi_1)^{2.5}(1-\phi_2)^{2.5}}\left[1+\frac{n-1}{d}(We)^d\left(\frac{1}{4}(f'')^d + (g')^d\right)\right]\left(\frac{1}{4}(f'')^2 + (g')^2\right) + \frac{k_f}{k_{hnf}}H_s Pr\theta = 0, \\ \theta(0)=1, \ \theta(\infty)=0 \end{array}\right\} \qquad (11)$$

Physical quantities.   The dimensionless parameters of present problem are defined as

$$Ec=\frac{xl(\Omega sin\alpha)^2}{(C_p)_f(T_0-T_w)}, \ \lambda=\frac{g(T_0-T_w)l\beta cos\alpha}{\Omega sin\alpha(\nu_f)^2}, \ M^2=\frac{B_0^2\sigma_{hnf}}{\rho_f\Omega sin\alpha},$$

$$Pr=\frac{\mu_f(C_p)_f}{k_f}, \ H_s=\frac{Q_0}{sin\alpha\Omega(\rho C_p)_f}, \ F_r=\frac{F_s x}{(k^*)^{1/2}}, \ \epsilon=\frac{\nu_f F_s}{\Omega sin\alpha}, \ N_r=\frac{k^* k_f}{4\sigma^*(T_\infty)^3}.$$

Shear stresses in view of y- and x-directions are expressed as

$$C_f = \frac{2\tau_{xz}|_{z=0}}{\rho_f(\Omega x \sin\alpha)^2}, C_g = \frac{2\tau_{yz}|_{z=0}}{\rho_f(\Omega x \sin\alpha)^2},$$

$$(Re)^{1/2}C_f = \frac{-1}{(1-\phi_1)^{2.5}(1-\phi_2)^{2.5}}\left[1 + \frac{n-1}{d}\left(We f''(0)\right)^d\right]f''(0),$$

$$(Re)^{1/2}C_g = \frac{-1}{(1-\phi_1)^{2.5}(1-\phi_2)^{2.5}}\left[1 + \frac{n-1}{d}\left(We g'(0)\right)^d\right]g'(0).$$

The Nusselt number is constructed as

$$Nu = \frac{xQ_w}{k_f(T-T_\infty)}, Q_w = -k_{hnf}\frac{\partial T}{\partial z},$$

$$(Re)^{-1/2}Nu = \frac{-k_{hnf}}{k_f}\theta'(0).$$

The local Reynolds number is $Re\left(= \frac{x^2\Omega \sin\alpha}{\nu_f}\right)$.

Numerical method for solution

Weighted residual Galerkin approach (WRGA) is implemented to simulate numerical values of Eqs. (9–11). Here, $f' = F$ is considered to formulate the required residuals. The following description is discussed below.

Division of problem domain. The domain of the problem is broken into 300 elements whereas weak forms are developed using the weighted residual integrals. Linear polynomial is made over each 300 elements of domain. Weights functions are multiplied along with residuals and integration is taken. The approximation computations of f, θ and F are defined below. So the weighted residuals described in[24,25,30,31,34] are

$$\int_{\eta_e}^{\eta_{e+1}} We\left[f' - F\right]d\eta = 0,$$

$$\int_{\eta_e}^{\eta_{e+1}} w_1 \left[\begin{array}{c} F'' + \frac{\nu_f}{\nu_{hnf}}\left(\frac{1}{2}(F)^2 - fF' - 2g^2 - 2\lambda\theta\right) \\ -\frac{M^2(1-\phi_1)^{2.5}(1-\phi_2)^{2.5}}{(1+\beta_e\beta_i)^2+\beta_e^2}\left[2\beta_e g + (1+\beta_e\beta_i)F\right] \\ +(We)^d\frac{(n-1)(d+1)}{d}F''(F')^d + \epsilon F - H_1 F_r(F)^2 \end{array}\right]d\eta = 0,$$

$$\int_{\eta_e}^{\eta_{e+1}} w_2 \left[\begin{array}{c} g'' + \frac{\nu_f}{\nu_{hnf}}\left(gf' - fg'\right) + (We)^d\frac{(n-1)(d+1)}{d}g''(g')^d - \epsilon g \\ -\frac{M^2(1-\phi_1)^{2.5}(1-\phi_2)^{2.5}}{(1+\beta_e\beta_i)^2+\beta_e^2}\left[-\frac{1}{2}\beta_e f' + (1+\beta_e\beta_i)g\right] - H_1 F_r\left(f'\right)^2 \end{array}\right]d\eta = 0,$$

$$\int_{\eta_e}^{\eta_{e+1}} w_3 \left[\begin{array}{c} g'' + \frac{\nu_f}{\nu_{hnf}}\left(gf' - f'g'\right) + (We)^d\frac{(n-1)(d+1)}{d}g''(g')^d - \epsilon g \\ -\frac{M^2(1-\phi_1)^{2.5}(1-\phi_2)^{2.5}}{(1+\beta_e\beta_i)^2+\beta_e^2}\left[-\frac{1}{2}\beta_e F + (1+\beta_e\beta_i)g\right] - H_1 F_r(F)^2 \end{array}\right]d\eta = 0,$$

$$\int_{\eta_e}^{\eta_{e+1}} w_4 \left[\begin{array}{c} (1+\epsilon\theta)\theta'' + \frac{k_f}{k_{hnf}}\frac{(\rho c_p)_{hnf}}{(\rho c_p)_f}Pr\left(\frac{1}{2}F\theta - f\theta'\right) + \frac{k_f}{k_{hnf}}H_s Pr\theta \\ + \frac{k_f}{k_{hnf}}\frac{PrEcM^2}{(1+\beta_e\beta_i)^2+\beta_e^2}\left(\frac{1}{4}(F)^2 + \left(g'\right)^2\right) \\ \frac{k_f}{k_{hnf}}\frac{PrEc}{(1-\phi_1)^{2.5}(1-\phi_2)^{2.5}}\left(\frac{1}{4}\left(F'\right)^2 + \left(g''\right)^2\right) \end{array}\right]d\eta = 0,$$

Here, w_1, w_2, w_3 and w_4 are weight functions. The unknown variables f, F, g and θ are considered as

$$f = \sum_{j=1}^{2} f_i\psi_j, F = \sum_{j=1}^{2} F_i\psi_j, \theta = \sum_{j=1}^{2} \theta_i\psi_j, g = \sum_{j=1}^{2} g_i\psi_j,$$

Assembly development. Assembly procedure plays a vital role for development of boundary vector, source vector and stiffness matrix. Further, it is used to generate the global stiffness matrix while Picard linearization approach makes linearization in non-linear equations. Hence, local stiffness elements are

$$K_{ij}^{11} = \int_{\eta_e}^{\eta_{e+1}} \psi_i\left(\frac{d\psi_j}{d\eta}\right)d\eta, K_{ij}^{12} = -\int_{\eta_e}^{\eta_{e+1}} \psi_i\left(\psi_j\right)d\eta, K_{ij}^{13} = 0, K_{ij}^{14} = 0, b_i^1 = 0,$$

$$K_{ij}^{21} = 0, K_{ij}^{23} = \int_{\eta_e}^{\eta_{e+1}} \left[\psi_j \psi_i 2\overline{g} + \frac{M^2(1-\phi_1)^{2.5}(1-\phi_2)^{2.5}}{(1+\beta_e\beta_i)^2 + \beta_e^2} 2\beta_e \psi_i(\psi_j) \right] d\eta,$$

$$K_{ij}^{22} = \int_{\eta_e}^{\eta_{e+1}} \left[\begin{array}{c} -\left(1 + +(We)^d \frac{(n-1)(d+1)}{d} \left(\overline{F'}\right)^d\right) \frac{d\psi_i}{d\eta} \frac{d\psi_j}{d\eta} \\ -\frac{M^2(1-\phi_1)^{2.5}(1-\phi_2)^{2.5}}{(1+\beta_e\beta_i)^2 + \beta_e^2} \left[(1+\beta_e\beta_i)\psi_j\psi_i\right] \\ +\epsilon\psi_j\psi_i - H_1 F_r \overline{H}\psi_j\psi_i + \frac{v_f}{v_{hnf}} \left(\frac{1}{2}\overline{H}\psi_j\psi_i - \overline{f}\psi_i \frac{d\psi_j}{d\eta}\right) \end{array} \right] d\eta,$$

$$K_{ij}^{24} = \int_{\eta_e}^{\eta_{e+1}} \left[-\frac{v_f}{v_{hnf}} \left(2\lambda\psi_j\psi_i\right) \right] d\eta, b_i^2 = 0, K_{ij}^{32} = 0, K_{ij}^{34} = 0,$$

$$K_{ij}^{33} = -\int_{\eta_e}^{\eta_{e+1}} \left[\begin{array}{c} -\left(1 + (We)^d \frac{(n-1)(d+1)}{d} \left(\psi_i \frac{d\psi_j}{d\eta}\right)^d\right) \frac{d\psi_i}{d\eta} \frac{d\psi_j}{d\eta} \\ -\frac{M^2(1-\phi_1)^{2.5}(1-\phi_2)^{2.5}}{(1+\beta_e\beta_i)^2 + \beta_e^2} \left[(1+\beta_e\beta_i)\right]\psi_j\psi_i - \epsilon\psi_j\psi_i \\ -H_1 F_r \overline{g}\psi_j\psi_i \end{array} \right] d\eta, b_i^3 = 0,$$

$$K_{ij}^{31} = -\int_{\eta_e}^{\eta_{e+1}} \left[\frac{M^2(1-\phi_1)^{2.5}(1-\phi_2)^{2.5}}{(1+\beta_e\beta_i)^2 + \beta_e^2} \frac{1}{2}\beta_e\psi_j\psi_i \right] d\eta, b_i^4 = 0,$$

$$K_{ij}^{44} = -\int_{\eta_e}^{\eta_{e+1}} \left[\begin{array}{c} -(1+\epsilon\theta)\frac{d\psi_i}{d\eta}\frac{d\psi_j}{d\eta} + \frac{k_f}{k_{hnf}}\frac{(\rho c_p)_{hnf}}{(\rho c_p)_f} Pr\left(\frac{1}{2}\overline{F}\psi_j\psi_i - \overline{f}\psi_i\frac{d\psi_j}{d\eta}\right) \\ +\frac{k_f}{k_{hnf}} H_s Pr\psi_j\psi_i \end{array} \right] d\eta,$$

$$K_{ij}^{41} = -\int_{\eta_e}^{\eta_{e+1}} \left[\frac{k_f}{k_{hnf}} \frac{PrEcM^2}{(1+\beta_e\beta_i)^2 + \beta_e^2} \frac{1}{4}\overline{F}\psi_j\psi_i + \frac{k_f}{k_{hnf}} \frac{PrEc}{(1-\phi_1)^{2.5}(1-\phi_2)^{2.5}} \overline{F'}\psi_i\frac{d\psi_j}{d\eta} \right] d\eta,$$

$$K_{ij}^{43} = -\int_{\eta_e}^{\eta_{e+1}} \left[\begin{array}{c} \frac{k_f}{k_{hnf}} \frac{PrEcM^2}{(1+\beta_e\beta_i)^2 + \beta_e^2} \frac{1}{4}\overline{g'}\psi_j\frac{d\psi_j}{d\eta} \\ -\frac{k_f}{k_{hnf}} \frac{PrEc}{(1-\phi_1)^{2.5}(1-\phi_2)^{2.5}} \frac{d\psi_i}{d\eta}\frac{d\psi_j}{d\eta} \end{array} \right] d\eta, K_{ij}^{41} = 0,$$

System of non-linear (algebraic equations) is modeled with help of assembly procedure.

$$Mt\left(f, f', \theta\right)\binom{f}{\theta} = [\dot{F}],$$

$\dot{F}$(force vector), Mt (global stiffness matrix) and force vector ($\dot{F}$) and unknown nodal values $\binom{f}{\theta}$.

Convergence analysis. The error is established as

$$E_{er} = |\chi^i - \chi^{i-1}|$$

and range of convergence is noticed as

$$Max|\chi^i - \chi^{i-1}| < 10^{-8}.$$

It is mentioned that system of linear equations is simulated iteratively according computational tolerance (10^{-8}).

Grid independent investigation. FEM code is designed in Maple 18 while [0, 8] is called computational domain. Table 2 is performed as grid independent analysis for 300 elements and solution becomes converge at mid of each 300 elements.

Validation of results. It is noticed that results of present problem is verified with published study by Malik et al.[32] considering $H_s = 0, M = 0.002, F_r = 0, \epsilon = 0, Ec = 0, Pr = 0.7, \beta_e = 0, \beta_i = 0, \phi_1 = 0, \phi_2 = 0$. (Table 3)

7

Number of elements	$f'\left(\frac{\eta_\infty}{2}\right)$	$g\left(\frac{\eta_\infty}{2}\right)$	$\theta\left(\frac{\eta_\infty}{2}\right)$
30	0.2397335394	0.05453547774	0.1933024653
60	0.2232020794	0.05200805054	0.1819254898
90	0.2177959068	0.05117858942	0.1782491777
120	0.2151131380	0.05076561105	0.1764321953
150	0.2135099778	0.05051829239	0.1753486293
180	0.2124439114	0.05035356891	0.1746289887
210	0.1875839826	0.04551373254	0.1595173162
240	0.2111142682	0.05014775377	0.1737326708
270	0.2106720780	0.05007924754	0.1734348231
300	0.2103180036	0.05002488541	0.1731961042

Table 2. Mesh-free simulations of velocities and temperature via 300 elements[34].

λ	Malik et al.[32]			present numerical values		
	$(Re)^{1/2}C_f$	$(Re)^{1/2}C_g$	$(Re)^{-1/2}Nu$	$(Re)^{1/2}C_f$	$(Re)^{1/2}C_g$	$(Re)^{-1/2}Nu$
0.0	1.0253	0.6153	0.4295	1.0248	0.6149	0.4291
1	2.2007	0.8492	0.6121	2.2003	0.8381	0.6130
10	8.5041	1.3990	1.0097	8.5039	1.3973	1.0088

Table 3. Validation of present results for skin friction coefficients and temperature gradient.
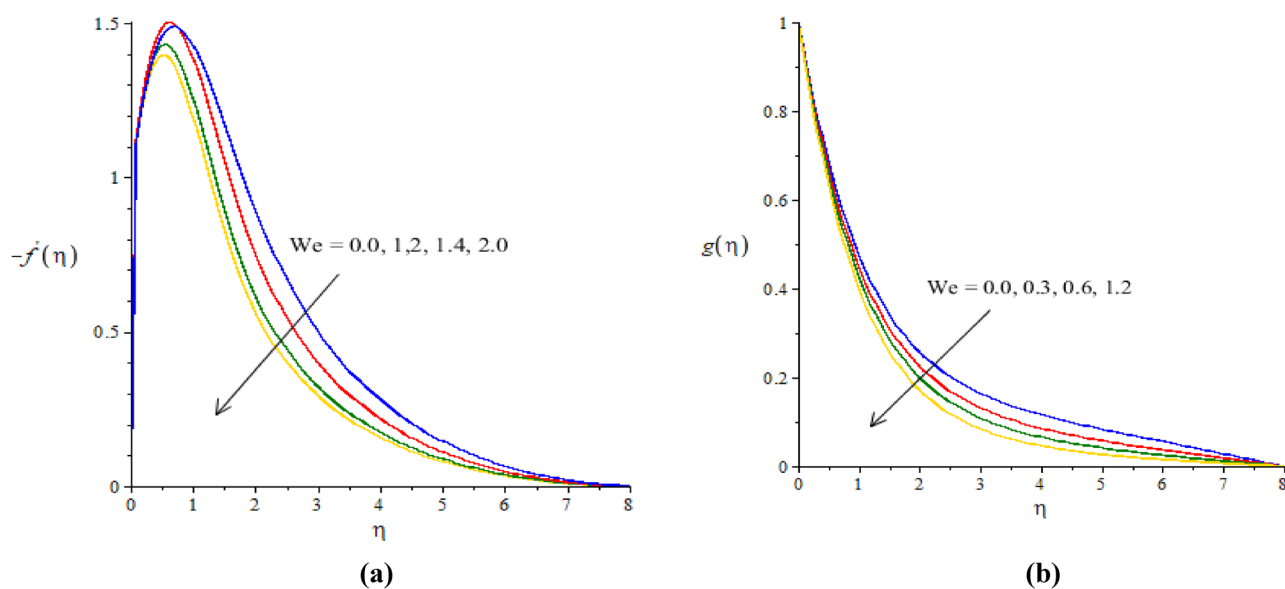
Figure 3. (**a, b**) The graphical view of velocities versus *We*.

Results and discussion

In this section, the characterizations of heat transport phenomena in Carreau Yasuda liquid carrying nanoparticles and hybrid nanoparticles over a porous heated cone. The transport of heat energy takes place in terms of thermal radiation and viscous dissipation under the action of ion slip and Hall forces. The strong technique is used to capture the results in terms of tables and graphs. The detail study of current model is addressed as:

Graphical simulations of fluid motion. The flow situation is verified against the variation of *We* (Weissenberg number), ion slip and Hall parameters (β_i, β_e) and Forchheimer number (F_r) by Figs. 3a,b, 4a,b, 5a,b, 6a,b. The role of *We* on the fluid motion is visualized by Fig. 3a,b. The decreasing function is investigated between the relation of *We* and motion of fluid particles. This decreasing function is plotted using the concept of Weissenberg number carrying the study of nanoparticles and hybrid nanoparticles. Physically, Weissenberg number has direct relation versus elastic force whereas Weissenberg number has inverse relation against viscous force. An increment in Weissenberg number creates more viscosity in fluid particles. More viscous fluid
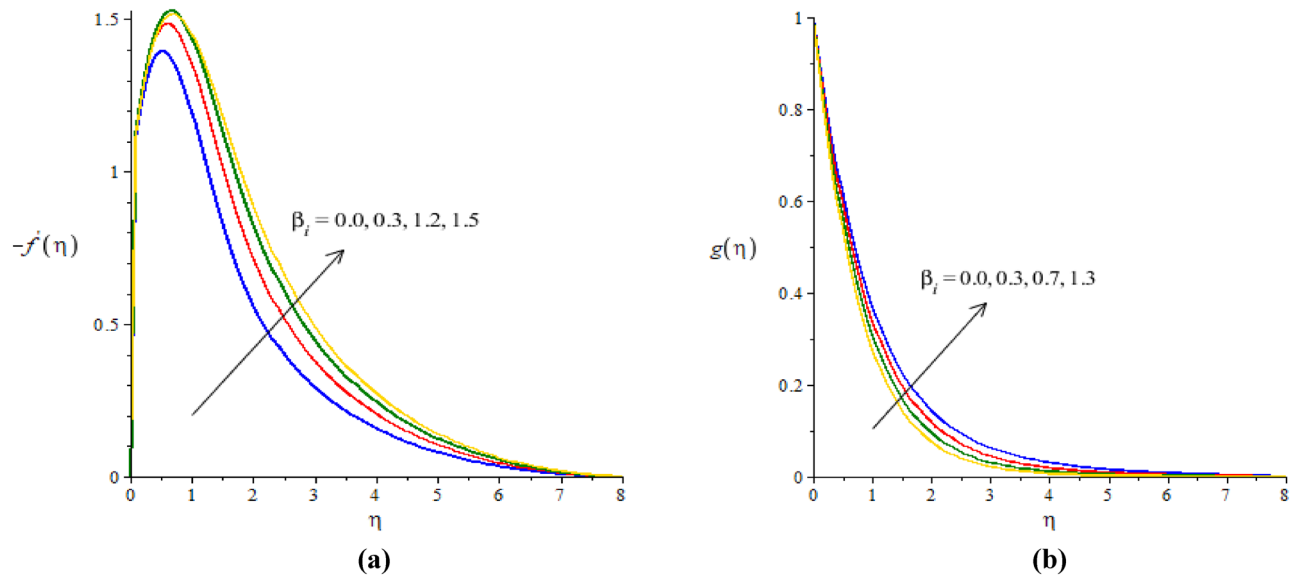
8

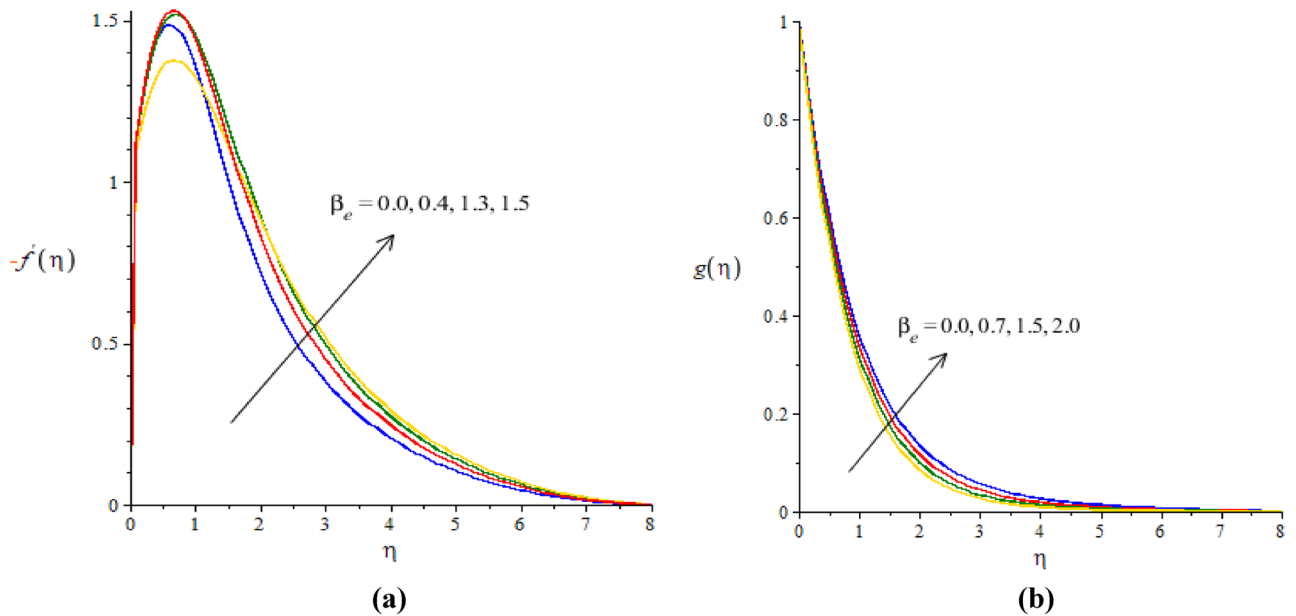**Figure 4.** (a,b) The graphical view of velocities versus β_i.

Figure 5. (a,b)The graphical view of velocities versus β_e.

is occurred against large values of Weissenberg number. Therefore, reduction in motion of nanoparticles and hybrid nanoparticles is captured. Figure 4a,b visualize the flow behavior versus the change in ion-slip number. It is noticed that β_i appears in momentum equations reveals the direct relation versus the motion of fluid particles. An increase in β_i results more enhancement in motion of fluid particles is occurred. So, ionization of particles is useful to develop speed in fluid particles. The concept of ion-slip parameter is formulated using generalized ohm's law. The collision due to ions into fluid particles is enhanced when ion-slip number is inclined. Further, ion-slip number has inverse relation with respect to Lorentz force. So, higher values of ion-slip number create reduction in Lorentz force. Reduction in Lorentz force makes an increment in motion of fluid particles. Hence, β_i is favorable number to obtain the maximum speed in motion of fluid particles. β_e is called Hall parameter and physical situation is taken out on the flow considering by Fig. 5a,b. Same situation is captured for the case of Hall parameter towards the motion in fluid particles. In physical point of view, Hall parameter has significant role on the motion of fluid particles. The fluid motion accelerates versus the impact of β_e. It is noticed that inverse relation is investigated among frictional magnetic force and Hall force. Lorentz force is also reduced versus higher values of Hall force. Such kinds of happenings are made reason for reduction into fluid motion. The distribution of F_r on the flow in view of vertical and horizontal directions is addressed by Fig. 6a,b. The primary and secondary flows are declined versus the change in F_r. F_r is modeled due to concept of Forchheimer porous media into
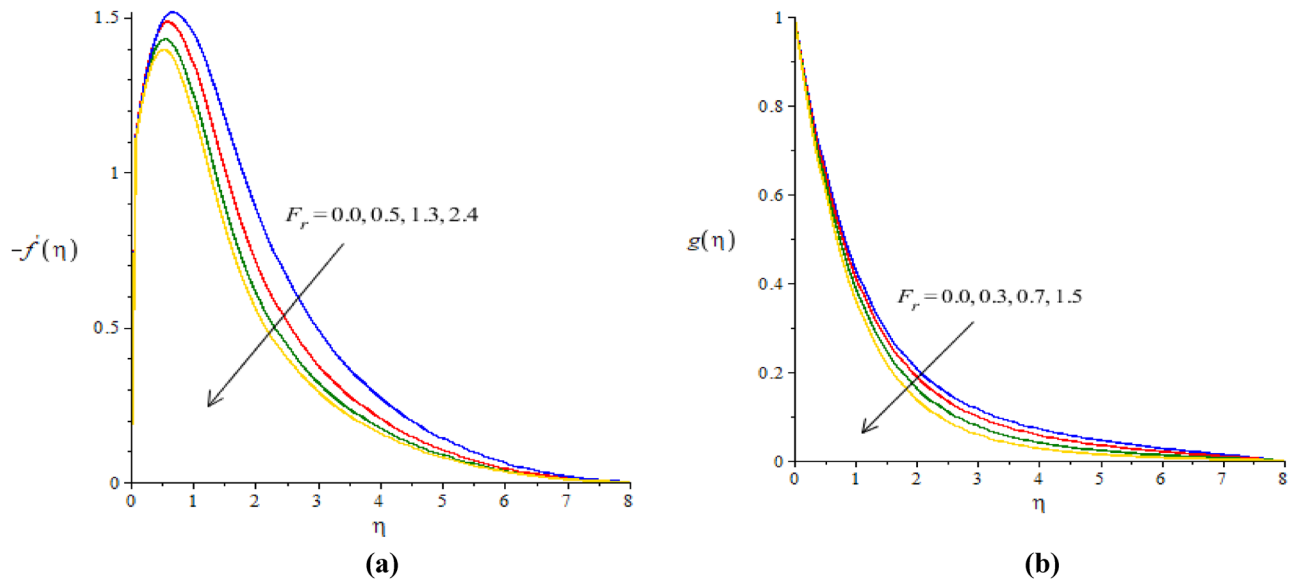
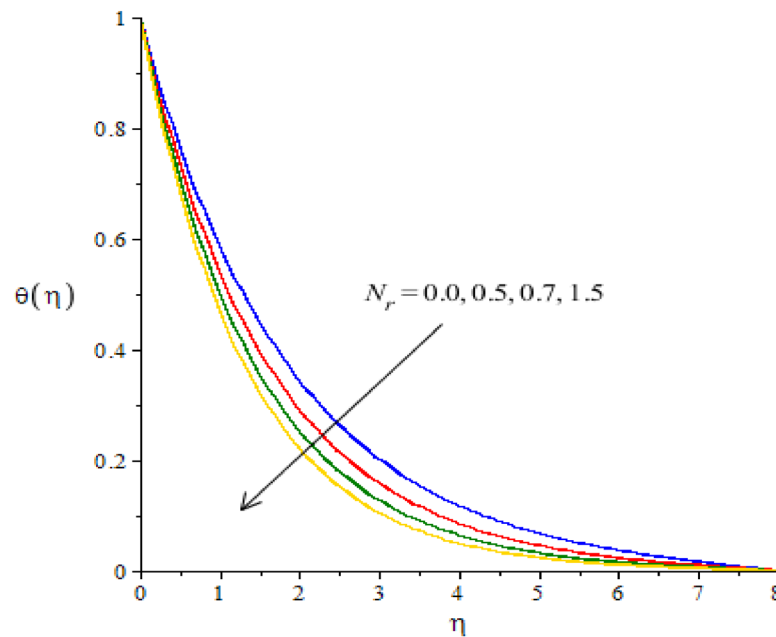**Figure 6.** (a,b) The graphical view of velocities versus F_r.

Figure 7. The graphical view of temperature versus N_r.

fluid particles. F_r is known as non-linear function versus the motion into fluid particles. The retardation force is formulated against the impact of F_r. This reduction is produced due to porous surface inserting the parameter F_r. Hence, decreasing trend is captured into the motion of fluid particles.

Graphical simulations of fluid temperature. The phenomenon of fluid temperature is addressed against the variation of $N_r, H_s, \beta_e, \beta_i$ and Ec. The graphical role of fluid temperature inserting nanoparticles and hybrid nanoparticles is measured by Figs. 7, 8, 9, 10 and 11. Figure 7 illustrates the behavior of N_r on the fluid temperature. In this plotting graph, the reduction is simulated in view of thermal energy. This reduction is created due to large values of thermal radiation number. Physically, heat energy moves away from the surface of cone in form of electromagnetic waves. By this impact, the reduction is occurred into heat energy of fluid particles. Moreover, inverse relation is modeled among thermal radiation and heat energy. Large values of thermal radiation number make reduction in heat energy of hybrid nanoparticles. The character of H_s versus the temperature profile is considered by Fig. 8. The large values of heat energy make the more production in heat energy while large amount of heat energy is made due to external heat source. Hence, external heat source makes the reason for obtaining the maximum production of heat energy. It is noticed that negative values of H_s
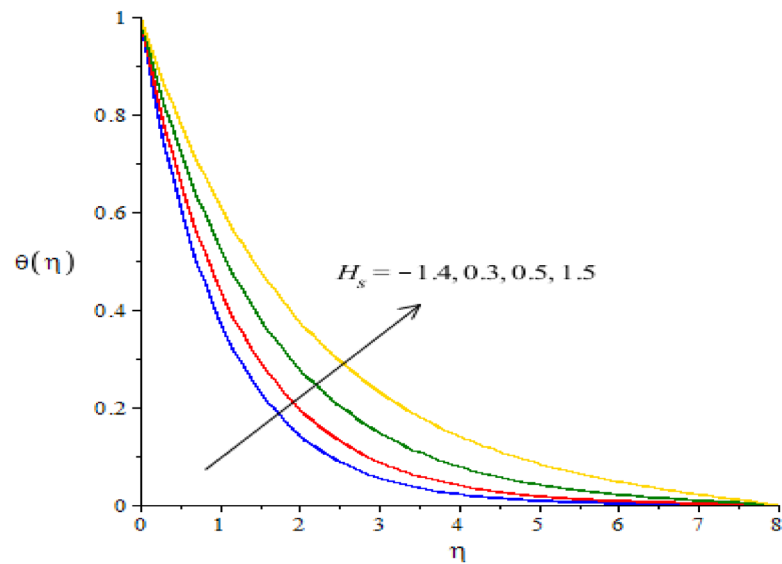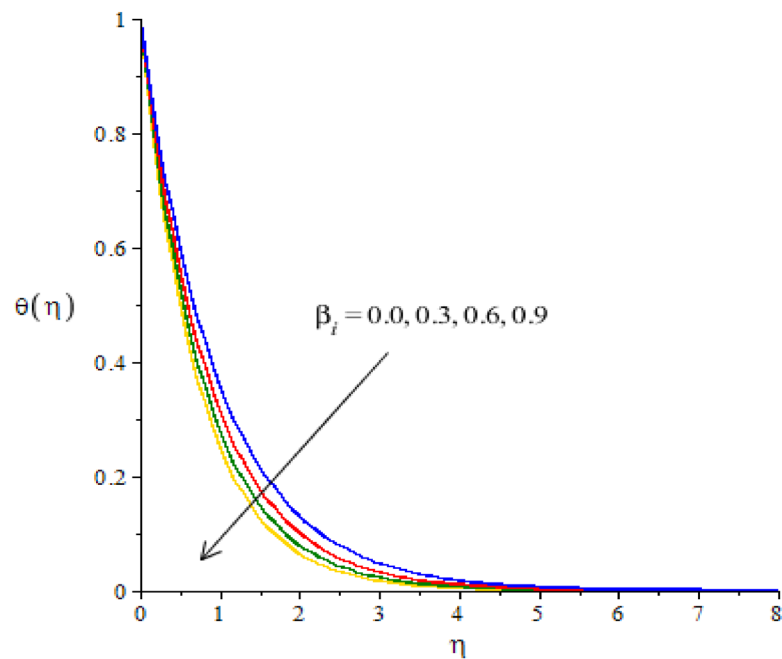
Figure 8. The graphical view of temperature versus H_s.

Figure 9. The graphical view of temperature versus β_i.

are taken due to heat absorption while positive values for H_s are indicated as concept of heat generation. More heat energy generates using the concept of external heat source. Figures 9 and 10 reveal the relation between fluid temperature and ion slip and Hall numbers. The production of heat energy is decreased via enlargement in ion slip and Hall numbers. It is estimated that ion slip and Hall numbers are appeared in energy equation. Moreover, the inverse relation is captured versus the existence of ion slip and Hall numbers. An increment in ion slip and Hall numbers brings the reduction in heat energy. It is mentioned that ion slip and Hall currents are formulated due to concept of Joule heating phenomena (in the attendance of generalized ohm's theory). Joule heating phenomena indicates inverse relation against ion slip and Hall currents. Hence, Joule heating is inclined using higher values of ion slip and Hall currents. MBLT (thickness of momentum boundary layers) are adjusted by varying values of ion slip and Hall currents. The motion of ions makes reduction in heat energy due to large values of ion slip and Hall numbers. The characterization of Ec is considered as an essential role for maximum achievement of thermal energy while this behavior is captured by Fig. 11. From mathematical view,
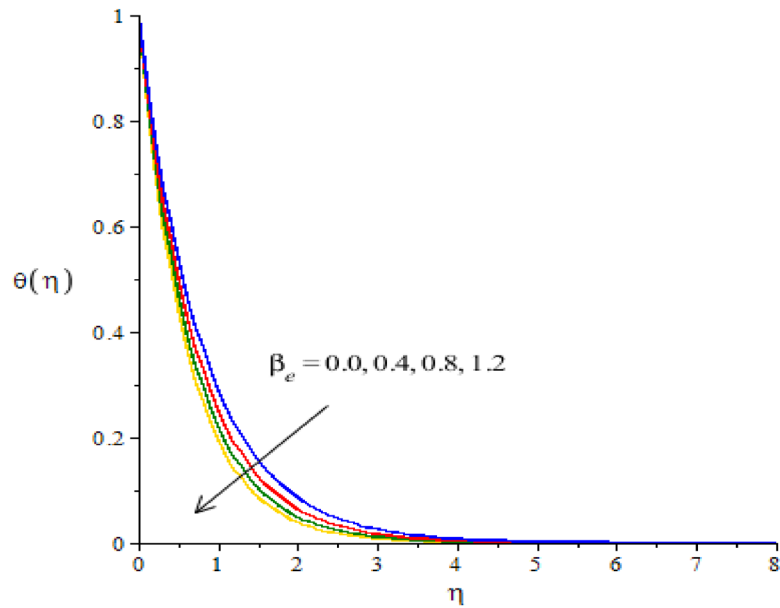
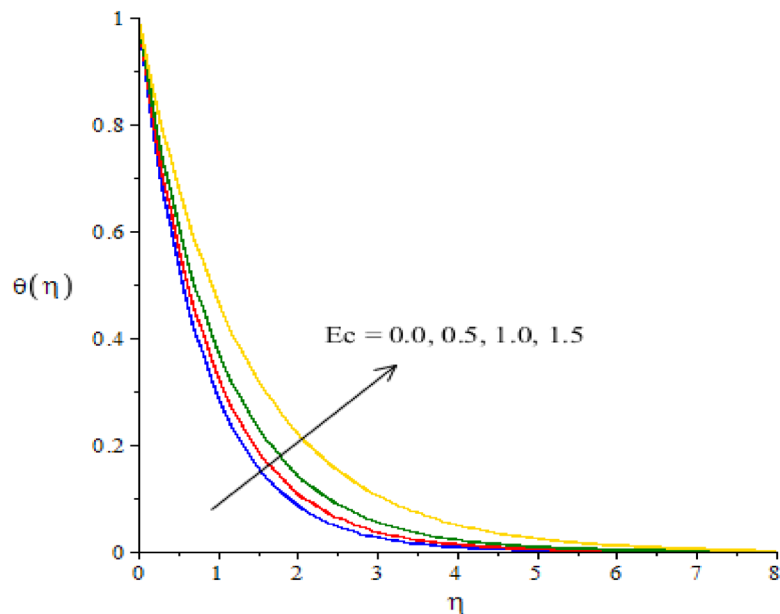**Figure 10.** The graphical view of temperature versus β_e.

Figure 11. The graphical view of temperature versus Ec.

Ec is appeared in energy equation (dimensionless). Hence, direct relation is investigated versus thermal energy. Physically, Ec is modeled due to viscous dissipation in energy equation. More viscous dissipation is developed inserting the role of Ec. Heat energy dissipates when viscous nature is occurred into fluid particles. Maximum heat energy is produced because of additional retarding force. Meanwhile, Ec is visualized as a useful parameter for developing more thermal energy.

Numerical treatment of surface force and Nusselt number. The surface force, temperature gradient and Sherwood number are visualized near the surface of cone. The numerical simulations of surface force, Nusselt number and rate of solute against change in $We, F_r, \beta_e, \beta_i$ and H_s are simulated. These numerical simulations are taken out by Table 4. The surface force is decreased via enlargement of heat generation, ion slip and Hall numbers but surface force called the skin friction coefficient is significantly enhanced considering variation of F_r. The production of rate of heat energy is increased versus the enhancement of Forchheimer, ion slip and Hall numbers. Therefore, Forchheimer, ion slip and Hall numbers play a vital impact for the enhancement of tem-

		$-(Re)^{1/2}C_f$	$-(Re)^{1/2}C_g$	$-(Re)^{-1/2}Nu$
	0.0	0.4998714299	0.6029282911	0.7104807445
We	0.3	0.8581100631	0.8821689645	0.7114238688
	0.5	2.698548989	0.9686090229	0.7121467218
	0.0	0.2864470301	0.7360866944	0.7111316028
Fr	0.7	0.2704802904	0.8166854253	0.7098459854
	1.3	0.2277144057	0.8787076034	0.7080141595
	0.0	0.2713783769	0.1613967311	0.7119591618
β_e	0.3	0.2680990013	0.13730063316	0.8132986239
	0.7	0.2398120967	0.02406085455	0.9137297415
	0.0	0.2753085726	0.2499991558	0.7122827047
β_i	0.4	0.1787392657	0.1207572825	0.8099581562
	0.8	0.0824121081	0.0860598593	0.9398457277
	-1.3	0.2826682046	0.7000830123	0.17668466241
H_s	0.0	0.1839467002	0.5539122359	0.36947614874
	1.2	0.00849283892	0.3058238772	0.71907271478

Table 4. Numerical values of gradient temperature and skin friction coefficients versus various parameters.

perature gradient. In case of heat generation number gradient temperature is reduced due to inserting the large values of heat generation number.

Key consequences of current model

The porous and rotating cone is used to visualize the impacts of ion slip and Hall forces in thermal energy mechanism considering Carreau Yasuda liquid. The phenomenon of heat transport is occurred in the presence of heat generation, nanoparticles, hybrid nanoparticles and thermal radiation. The numerical scheme (FEM) is used to simulate the numerical results. The prime consequences discussed below.

- Hall and ion slip parameters are considered significant parameters to produce the enhancement in motion of fluid particles but speed of nano and hybrid nanoparticles becomes slow down versus large values of Forchheimer and Weissenberg numbers;
- An enhancement in production of heat energy is addressed via large values of heat generation number and Eckert number while reduction in heat energy is occurred due to positive values of thermal radiation and Hall and ion slip parameters;
- The convergence analysis is simulated via 300 elements;
- The temperature gradient is enhanced against the enhancement in Forchheimer, ion slip and Hall parameters but reverse behavior in noticed for the case of heat generation number;
- Surface force is improved neat wall of cone with respect to variation in Forchheimer number. Surface force is declined via higher values of heat generation and ion slip and Hall parameters;
- Dimensionless stresses and heat transfer coefficient varies directly against Weissenberg parameter.

Data availability

The datasets generated/produced during and/or analyzed during the current study/research are available from the corresponding author on reasonable request.

References

1. Mahmood, R. *et al.* A comprehensive finite element examination of Carreau Yasuda fluid model in a lid driven cavity and channel with obstacle by way of kinetic energy and drag and lift coefficient measurements. *J. Market. Res.* **9**(2), 1785–1800 (2020).
2. Boyd, J., Buick, J. M. & Green, S. Analysis of the Casson and Carreau-Yasuda non-Newtonian blood models in steady and oscillatory flows using the lattice Boltzmann method. *Phys. Fluids* **19**(9), 103 (2007).
3. Coclite, A., Coclite, G. M. & De Tommasi, D. Capsules rheology in Carreau-Yasuda Fluids. *Nanomaterials* **10**(11), 2190 (2020).
4. Pinarbasi, A. H. M. E. T. & Liakopoulos, A. Stability of two-layer poiseuille flow of Carreau-Yasuda and Bingham-like fluids. *J. Nonnewton. Fluid Mech.* **57**(2–3), 227–241 (1995).
5. Waqas, H., Khan, S. U., Bhatti, M. M. & Imran, M. Significance of bioconvection in chemical reactive flow of magnetized Carreau-Yasuda nanofluid with thermal radiation and second-order slip. *J. Therm. Anal. Calorim.* **140**(3), 1293–1306 (2020).
6. Hayat, T., Ullah, S., Khan, M. I. & Alsaedi, A. On framing potential features of SWCNTs and MWCNTs in mixed convective flow. *Results Phys.* **8**, 357–364 (2018).
7. Nayak, M. K., Shaw, S. & Chamkha, A. J. 3D MHD free convective stretched flow of a radiative nanofluid inspired by variable magnetic field. *Arab. J. Sci. Eng.* **44**(2), 1269–1282 (2019).
8. Hady, F. M., Eid, M. R. & Ahmed, M. A. A nanofluid flow in a non-linear stretching surface saturated in a porous medium with yield stress effect. *Appl Math Inf Sci Lett* **2**(2), 43–51 (2014).

13

9. Shafique, Z., Mustafa, M. & Mushtaq, A. Boundary layer flow of Maxwell fluid in rotating frame with binary chemical reaction and activation energy. *Results Phys.* **6**, 627–633 (2016).
10. Rehman, A. U., Mehmood, R., Nadeem, S., Akbar, N. S. & Motsa, S. S. Effects of single and multi-walled carbon nano tubes on water and engine oil based rotating fluids with internal heating. *Adv. Powder Technol.* **28**(9), 1991–2002 (2017).
11. Seth, G. S., Mishra, M. K. & Tripathi, R. Modeling and analysis of mixed convection stagnation point flow of nanofluid towards a stretching surface: OHAM and FEM approach. *Comput. Appl. Math.* **37**(4), 4081–4103 (2018).
12. Kandasamy, R., Mohamad, R. & Ismoen, M. Impact of chemical reaction on Cu, Al_2O_3 and SWCNTs–nanofluid flow under slip conditions. *Eng. Sci. Technol. Int. J.* **19**(2), 700–709 (2016).
13. McCash, L. B., Akhtar, S., Nadeem, S., Saleem, S. & Issakhov, A. Viscous flow between two sinusoidally deforming curved concentric tubes: advances in endoscopy. *Sci. Rep.* **11**(1), 1–8 (2021).
14. Zidan, A. M. *et al.* Entropy generation for the blood flow in an artery with multiple stenosis having a catheter. *Alex. Eng. J.* **60**(6), 5741–5748 (2021).
15. Saleem, A., Akhtar, S., & Nadeem, S. Bio-mathematical analysis of electro-osmotically modulated hemodynamic blood flow inside a symmetric and nonsymmetric stenosed artery with joule heating. *Int. J. Biomath.* 2150071 (2021)
16. McCash, L. B., Akhtar, S., Nadeem, S. & Saleem, S. Entropy analysis of the peristaltic flow of hybrid nanofluid inside an elliptic duct with sinusoidally advancing boundaries. *Entropy* **23**(6), 732 (2021).
17. Rehman, A., Hussain, A. & Nadeem, S. Assisting and opposing stagnation point pseudoplastic nano liquid flow towards a flexible Riga sheet: a computational approach. *Math. Probl. Eng.* **2021**, 6610332. https://doi.org/10.1155/2021/6610332 (2021).
18. Akhtar, S., McCash, L. B., Nadeem, S., Saleem, S. & Issakhov, A. Convective heat transfer for peristaltic flow of SWCNT inside a sinusoidal elliptic duct. *Sci. Prog.* **104**(2), 00368504211023683 (2021).
19. Rizwana, R., Hussain, A. & Nadeem, S. Mix convection non-boundary layer flow of unsteady MHD oblique stagnation point flow of nanofluid. *Int. Commun. Heat Mass Transf.* **124**, 105285 (2021).
20. Yasin, A., Ullah, N., Saleem, S., Nadeem, S. & Al-Zubaidi, A. Impact of uniform and non-uniform heated rods on free convective flow inside a porous enclosure: finite element analysis. *Phys. Scr.* **96**(8), 085203 (2021).
21. Ahmad, S., Nadeem, S. & Khan, M. N. Mixed convection hybridized micropolar nanofluid with triple stratification and Cattaneo-Christov heat flux model. *Phys. Scr.* **96**(7), 075205 (2021).
22. Yasin, A., Ullah, N., Nadeem, S. & Saleem. Finite element simulation for free convective flow in an adiabatic enclosure: Study of Lorentz forces and partially thermal walls. Case Studies in Thermal Engineering, 25, p.100981 (2021).
23. Hussain, A. *et al.* A combined convection carreau–yasuda nanofluid model over a convective heated surface near a stagnation point: a numerical study. *Math. Probl. Eng.* **2021**, 6665743. https://doi.org/10.1155/2021/6665743 (2021).
24. Nazir, U., Sadiq, M. A. & Nawaz, M. Non-Fourier thermal and mass transport in hybridnano-Williamson fluid under chemical reaction in Forchheimer porous medium. *Int. Commun. Heat Mass Transf.* (2021).
25. Nazir, U., Saleem, S., Nawaz, M. & Alderremy, A. A. Three-dimensional heat transfer in nonlinear flow: a FEM computational approach. *J. Therm. Anal. Calorim.* **140**(5), 2519–2528 (2020).
26. Abdelsalam, S. I. & Sohail, M. Numerical approach of variable thermophysical features of dissipated viscous nanofluid comprising gyrotactic micro-organisms. *Pramana: J. Phys.* **94**(1), 1–12 (2020).
27. Sohail, M. *et al.* Computational exploration for radiative flow of Sutterby nanofluid with variable temperature-dependent thermal conductivity and diffusion coefficient. *Open Physics* **18**(1), 1073–1083 (2020).
28. Bilal, S., Sohail, M. & Naz, R. Heat transport in the convective Casson fluid flow with homogeneous-heterogeneous reactions in Darcy-Forchheimer medium. *Multidiscip. Model. Mater. Struct.* **15**(6), 1170–1189 (2019).
29. Sohail, M. *et al.* Utilization of updated version of heat flux model for the radiative flow of a non-Newtonian material under Joule heating: OHAM application. *Open Phys.* **19**(1), 100–110 (2021).
30. Nazir, U., Saleem, S., Nawaz, M., Sadiq, M. A. & Alderremy, A. A. Study of transport phenomenon in Carreau fluid using Cattaneo-Christov heat flux model with temperature dependent diffusion coefficients. *Phys. A: Stat. Mech. Appl.* **554**, 1239921 (2020).
31. Abdelmalek, Z., Nazir, U., Nawaz, M., Alebraheem, J. & Elmoasry, A. Double diffusion in Carreau liquid suspended with hybrid nanoparticles in the presence of heat generation and chemical reaction. *Int. Commun. Heat Mass Transf.* **119**, 104932 (2020).
32. Malik, M. Y. *et al.* Mixed convection dissipative viscous fluid flow over a rotating cone by way of variable viscosity and thermal conductivity. *Results in physics* **6**, 1126–1135 (2016).
33. Saleem, S. & Nadeem, S. Theoretical analysis of slip flow on a rotating cone with viscous dissipation effects. *J. Hydrodyn. Ser. B* **27**(4), 616–623 (2015).
34. Nazir, U., Nawaz, M. & Alharbi, S. O. Thermal performance of magnetohydrodynamic complex fluid using nano and hybrid nanoparticles. *Phys. A Stat. Mech. Appl.* **553**, 124 (2020).

Acknowledgements

Author contributions

(1) U.N. and M.S. developed the model and write up the modelling section. (2) Solution methodology section is updated by U.N. (3) U.N. and M.M.S. draw the graphs. (4) Introduction section is updated by M.M.S., H.A. and P.K. in the revised draft. (5) H.A. and P.K. confirms the modelling and helped in the literature survey. (6) Results and discussion section is improved by M.S., M.M.S. and H.A. (7) M.M.S. and P.K. wrote the discussion section of the revised article. (8) Conclusion section is updated by M.S., H.A. and P.K.

Competing interests

The authors declare no competing interests.

Additional information

Correspondence and requests for materials should be addressed to M.S. or P.K.

Reprints and permissions information is available at www.nature.com/reprints.

Publisher's note Springer Nature remains neutral with regard to jurisdictional claims in published maps and institutional affiliations.